THE JOURNAL OF BIOLOGICAL CHEMISTRY VOL. 287, NO. 13, pp. 10368–10378, March 23, 2012

The Transmembrane Prolines of the Mitochondrial ADP/ATP Carrier Are Involved in Nucleotide Binding and Transport and Its Biogenesis*

Received for publication, November 8, 2011, and in revised form, January 27, 2012 Published, JBC Papers in Press, February 9, 2012, DOI 10.1074/jbc.M111.320697

Marion Babot[‡§1], **Corinne Blancard**[‡§], **Ludovic Pelosi**[¶], **Guy J.-M. Lauquin**[‡§], **and Véronique Trézéguet**[‡§2]

From the [‡]*Laboratoire de Physiologie Moléculaire et Cellulaire, Université de Bordeaux, the* [§]*CNRS, IBGC, UMR 5095, F-33000 Bordeaux, France and the* [¶]*Université Joseph Fourier, Equipe Dynamique des Organelles et Plasticité Cellulaire, Laboratoire de Biologie à Grande Echelle (BGE), iRTSV-CEA de Grenoble, 17 rue des Martyrs, F-38054 Grenoble cedex 9, France*

Background: The role of prolines in transmembrane helices (TMH) of mitochondrial ADP/ATP carrier is investigated.
Results: They play the role of hinges during nucleotide transport and biogenesis.
Conclusion: Pro-kinks in TMH allow carrier plasticity and biogenesis.
Significance: TMH proline mutations induce deleterious effects in ADP/ATP carrier import and in mitochondrial biogenesis.

The mitochondrial ADP/ATP carrier (Ancp) is a paradigm of the mitochondrial carrier family, which allows cross-talk between mitochondria, where cell energy is mainly produced, and cytosol, where cell energy is mainly consumed. The members of this family share numerous structural and functional characteristics. Resolution of the atomic structure of the bovine Ancp, in a complex with one of its specific inhibitors, revealed interesting features and suggested the involvement of some particular residues in the movements of the protein to perform translocation of nucleotides from one side of the membrane to the other. They correspond to three prolines located in the odd-numbered transmembrane helices (TMH), Pro-27, Pro-132, and Pro-229. The corresponding residues of the yeast Ancp (Pro-43, Ser-147, and Pro-247) were mutated into alanine or leucine, one at a time and analysis of the various mutants evidenced a crucial role of Pro-43 and Pro-247 during nucleotide transport. Beside, replacement of Ser-147 with proline does not inactivate Ancp and this is discussed in view of the conservation of the three prolines at equivalent positions in the Ancp sequences. These prolines belong to the signature sequences of the mitochondrial carriers and we propose they play a dual role in the mitochondrial ADP/ATP carrier function and biogenesis. Unexpectedly their mutations cause more general effects on mitochondrial biogenesis and morphology, as evidenced by measurements of respiratory rates, cytochrome contents, and also clearly highlighted by fluorescence microscopy.

The mitochondrial ADP/ATP carrier (Ancp),[3] localized in the mitochondrial inner membrane (MIM), is a key energetic link between cytosol and mitochondria as it provides the mitochondrial ATP synthase with its substrate, ADP or ATP, according to the cell physiological conditions, in exchange for the reaction product. Ancp is the paradigm of the mitochondrial carrier family (MCF) and its atomic structure was solved at high resolution in 2003 (1). It has been since used for homology modeling of other members of the MCF (2–6).

Although the three-dimensional structure of the bovine Anc1p (BfAnc1p) is that of an inhibited carrier, we could learn a lot from it. However, it is now necessary to go further to get insights into the precise mechanism of the nucleotide exchange. Ancp is very specifically and efficiently inhibited by two classes of inhibitors whose representative members are carboxyatractyloside (CATR) for one class, and bongkrekic acid (BA) for the other one. CATR binds only to the cytosolic side of the ADP/ATP carrier, whereas BA binds only to the matrix side. The extensive use of these inhibitors for past studies allowed to propose that they stabilize Ancp in two different conformations, named BA and CATR conformations, which are probably involved in the nucleotide exchange process. The three-dimensional structure of the BfAnc1p is that of the CATR conformation but that of the BA conformation is still missing. As a general rule membrane transporters are characterized by the switch from one conformation open to one side of the membrane to another one open to the opposite side of the membrane to catalyze transport.

In the BfAnc1p structure, the cavity is oriented toward the intermembrane space (IMS) and CATR lies deeply inside. The six-tilted TMH of BfAnc1p (TMH1 to 6) delineate this cavity. We can hypothesize that in the BA conformation, it is open toward the matrix and closed to the intermembrane space. The odd-numbered TMH are sharply kinked at the level of prolines. They belong to the signature sequences of the MCF members,

* This work was supported in part by the Université Bordeaux Segalen, the Centre National de la Recherche Scientifique, and the Région Aquitaine.
[1] Supported by the French Ministère de l'Enseignement Supérieur et de la Recherche.
[2] To whom correspondence should be addressed: CBMN, UMR 5248, Allée Geoffroy Saint-Hilaire Bât B14bis, 33600 Pessac, France. Tel: 33-5-4000-6847; Fax: 33-5-4000-2200; E-mail: v.trezeguet@cbmn.u-bordeaux.fr.
[3] The abbreviations used are: Ancp, adenine nucleotide carrier protein (ADP/ATP carrier); *ANC*, mitochondrial adenine nucleotide carrier (ADP/ATP carrier) encoding gene; ATR, atractyloside; BfAnc1p, isoform 1 of bovine Ancp; BA, bongkrekic acid; CATR, carboxyatractyloside; EMA, eosin-5-maleimide; IMS, inter membrane space; MCF, mitochondrial carrier family; MIM, mitochondrial inner membrane; N-ADP, naphthoyl ADP; ScAnc2p, isoform 2 of *S. cerevisiae* Ancp; SGal-W, synthetic galactose-containing minimal medium, with all amino acids but W; TMH, transmembrane helix; UCP2, isoform 2 of uncoupling protein; Ap_5A, P_1,P_5-di(adenosine-5′)-pentaphosphate; FCCP, carbonyl cyanide *p*-trifluoromethoxyphenylhydrazone.

A) YEAST MCF

MOTIF 1 IN H1	**P**	**X**	**[D/E]**	**X**	**X**	**[K/R]**
% CONSERVATION	*97*		*100*			*100*
ScAnc1p, 2 & 3	**P**	**I**	**E**	**R**	**V**	**K**
YMR166C	S	L	D	T	V	K
MOTIF 2 IN H3	**P**	**X**	**[D/E]**	**X**	**X**	**[K/R]**
% CONSERVATION	*85*		*79*			*91*
ScAnc1p, 2 & 3	**S**	**L**	**D**	**Y**	**A**	**R**
YLR348C	F	A	D	V	V	N
YMR241W	T	V	E	I	T	R
YIL134W	P	I	W	V	I	K
YBR192W	P	I	W	I	I	K
YEL006W	P	I	W	V	V	K
YIL006W	P	I	W	V	V	K
YKL120W	P	L	F	L	V	K
YDL119C	P	I	T	V	I	K
YPR128C	P	M	A	V	V	A
MOTIF 3 IN H5	**P**	**X**	**[D/E]**	**X**	**X**	**[K/R]**
% CONSERVATION	*100*		*91*			*91*
ScAnc1p, 2 & 3	**P**	**L**	**D**	**T**	**V**	**R**
YNL083W	P	I	N	L	L	R
YIL134W	P	F	Q	L	L	K
YPR128C	P	L	I	V	A	K
YKL120W	P	W	D	V	I	L
YER053C	P	A	D	V	M	V
YJR077C	P	A	D	T	L	L

B) Ancp SEQUENCES

MOTIF 1 in BAnc1p	**V**	**A**	**P**	**I**	**E**	**R**	**V**	**K**
%	*57*	*95*	*99*	*98*	*99*	*100*	*95*	*99*
OTHER RESIDUES	A	S	S	L	K	-	I	Q
%	43	5	1	2	1		5	1
MOTIF 2 in BAnc1p	V	Y	P	L	D	F	A	R
%	*100*	*100*	*57*	*100*	*99*	*61*	*89*	*100*
OTHER RESIDUES			S		X	Y	T/V/S	
%			43		1	39	11	
MOTIF 3 in BAnc1p	S	Y	P	F	D	T	V	R
%	*99*	*100*	*100*	*47*	*100*	*99*	*87*	*100*
OTHER RESIDUES	C			L		S	I/L	
%	1			49		1	13	

FIGURE 1. **Conservation of the mitochondrial carrier signature sequence (*A*) among the 34 members of the *S. cerevisiae* MCF and (*B*) among the mitochondrial ADP/ATP carriers.** Sequences were aligned using ClustalX (46). In *A,* the consensus sequences of the three motives (one-letter amino acid code) are shown, and shown below, the carriers for which the sequences are divergent. *ScAnc1p*, *-2*, and *-3*, mitochondrial ADP/ATP carrier isoforms 1, 2, and 3 (locus tags YR056c, YBL030c, YBR085w). The locus tags are defined in the *Saccharomyces* Genome Database. *B,* residues i-1 and i-2 of the consensus prolines are also represented. Occurrences of the residues are indicated as percent of the 114 Ancp sequences analyzed (30). The amino acid immediately after the motif 3 proline corresponds to Trp instead of Phe or Leu in 4% of the Ancp sequences.

P*X*(D/E)*XX*(K/R) (7, 8). An example of the conservation of these sequences is given for the *Saccharomyces cerevisiae* MCF (Fig. 1*A*). As can be seen these prolines are particularly well conserved: 97, 85, and 100% in TMH1, -3, and -5, respectively. Motif 2 is the less well conserved, but still relatively high.

In the case of the Ancp subfamily, it was suggested that the three transmembrane prolines play the role of hinges during the swing from one conformation to the other involved in nucleotide transport (1, 9). Although prolines in TMH1 and -5 of Ancp are perfectly conserved, the proline in TMH3 is replaced with a serine residue in almost 50% of Ancp sequences (Fig. 1*B*). However, Gray and Matthews (10) noticed in a survey of known protein structures that serine in helices has a high propensity to make hydrogen bonds to carbonyl oxygen atoms in the preceding turn of the helix. Ballesteros *et al.* (11) analyzed the structure of four membrane proteins and showed that the presence of serine in TMH can induce or stabilize a bending angle 3–4° wider than with alanine, potentially resulting in significant conformational changes across TMH. Indeed, TMH3 of ScAnc2p is also kinked at the level of this residue in the three-dimensional structure obtained by homology modeling (12).

Molecular dynamic simulations of the bovine ADP/ATP carrier in the presence of ADP reinforced the putative role of the transmembrane prolines. In these experiments, Wang and Tajkhorshid (13) probed early structural changes, which might be involved in substrate translocation. They observed on the nanosecond time scale radial, outward displacements of the C-terminal part of the odd numbered helices around Pro-27, Pro-132, and Pro-229 (in TMH1, -3, and -5, respectively), accompanied by rearrangements of the salt bridge network responsible for the closure of the bottom of the cavity. Besides, hydrogen/deuterium exchange kinetics coupled to mass spectrometry highlighted dramatic accessibility to the solvent of the regions exposed to the matrix and to the intermembrane space depending on the inhibitor bound to BfAnc1p, CATR, or BA (14), in line with conformational dynamics during the transport. For example, regions 21–35 in TMH1 and 129–140 in TMH3, encompassing MCF motives 1 and 2, were much more deuterated in the BA-carrier complex than in the CATR-carrier complex.

Besides, these prolines are part of the signature sequences of the MCF members, P*X*(D/E)*XX*(K/R), which were suggested to be involved in mitochondrial carrier biogenesis (15–17). Convincing experimental data are still missing. In addition, it was shown that other parts of the carriers participate in the translocation, namely TMH4 and part of TMH5 (18–21). Therefore we also investigated the role of these prolines in the mitochondrial import.

To do so, we mutated the positions of ScAnc2p equivalent to Pro-27, Pro-132, and Pro-229 (Pro-43, Ser-147, and Pro-247) either in a small amino acid, alanine, or in a bulkier hydrophobic one, leucine. Alanine scanning was often used to probe important residues for protein function (22, 23). Leucine is considered a helix former and stabilizer (24) and we can expect negative effects on transport activity if these three prolines act as hinges for helix movements to close or open the Ancp cavity during nucleotide translocation. Genetic studies are easier with yeast than with bovine. ScAnc2p was chosen because it is the only isoform necessary for *S. cerevisiae* to grow under respiratory conditions (25). Furthermore, primary sequence conservation is relatively high between the bovine and yeast carriers (47% identity) indicating that any conclusion drawn for the yeast carrier will be accurate for the bovine carrier.

As expected, proline/serine substitutions hampered ScAnc2p activity, although at very different levels. Interestingly, the productive ADP binding to Ancp as well as CATR binding properties were modified. Noticeably, the consequences of Pro-43, Ser-147, and Pro-247 mutations were also at the mitochondrial level: oxygen consumption, cytochrome

contents, morphology, and network. Hence, we evidenced for the first time a role of Ancp in its own biogenesis and more generally in mitochondrial biogenesis, in line with Ancp being a key energetic link in the cell metabolism. Ancp not only provides the cell with its main energy source but also controls the quality and the amount of the organelle that produces this energy and hosts Ancp.

EXPERIMENTAL PROCEDURES

Chemicals—[^{3}H]Atractyloside ([^{3}H]ATR) and N-ADP were synthesized as previously described in David *et al.* (12). Protein concentration was determined using the bicinchoninic acid reagent kit from Sigma. Nucleotides and CATR were purchased from Sigma, and Ap_5A from Calbiochem. The hexokinase/glucose-6-phosphate dehydrogenase enzyme mixture was obtained from Roche Diagnostics GmbH.

Strains, Media, and Transformation—Escherichia coli strain used for plasmid propagation was XL1-Blue (*recA1 endA1 gyrA96* (*Nal*^{r}) *thi hsdR17* (r_K^- m_K^+) *supE44 relA1 lac*$^-$ *F′* [*Tn10* (*tet*^{r}) *proAB*$^+$ *lacI*^{q} *lacZ*Δ*M15*]). Bacteria were transformed according to standard methods either with calcium chloride or by electroporation, as already described in De Marcos Lousa *et al.* (26). The following *Saccharomyces cerevisiae* strains were used in this study: *JL1*Δ*2*Δ*3u*$^-$ (*MATa leu2–3,112 his3–11,15 ade2-1 trp1-1 ura3-1 can1–100 anc1*::*LEU2* Δ*anc2*::*HIS3* Δ*anc3*) (12). The strains were grown and transformed as described in De Marcos Lousa *et al.* (26). The composition of all the media used (YPD, YPLact, and SGal-W) is described in Ref. 26.

Site-directed Mutagenesis—Site-directed mutagenesis of *ScANC2* was performed using the Transformer^{TM} Site-directed Mutagenesis Kit (Clontech) with the following mutagenic primers (mutated bases are underlined and amino acid substitution is indicated in parentheses): 5′-^{118}GCTGCATCTGCCATCGAAAGAG^{139}-3′ (P43A); 5′-^{118}GCTGCATCTCTAATCGAAAGAG^{139}-3′ (P43L); 5′-^{427}CTATTTGTTTACCCTTGGATTATG^{451}-3′ (S147P); 5′-^{427}CTATTTGTTTACGCCTTGGATTATG^{451}-3′ (S147A); 5′-^{427}CTATTTGTTTACTTGTTGGATTATG^{451}-3′ (S147L); 5′-^{731}GTTCTTACGCTTTGGATACC^{750}-3′ (P247A); 5′-^{731}GTTCTTACTTATTGGATACC^{750}-3′ (P247L).

The mutated *ScANC2* genes were subcloned into a centromeric plasmid, pRS314 under the control of *ScANC2* regulatory sequences as described in Ref. 12. The resulting plasmids were used to transform the *JL1*Δ*2*Δ*3u*$^-$ strain to assess their ability to complement the *Scanc2* deletion.

Cell Cytochrome Contents—Cells were cultivated in 100 ml of SGal-W until their $A_{600\,nm}$ = 2–4. Cells were harvested and washed twice with fresh water, then resuspended in 10 mM potassium P_i, pH 6.8 ($A_{600\,nm} \approx 100$). They were reduced with sodium dithionite and oxidized with 10 μl/ml of 3% H_2O_2. Measurements and quantification were then performed as described in Ref. 26.

Yeast Cell Extracts—Cell proteins were extracted by the post-alkaline method described by Kushnirov (27). Briefly, cells were grown in SGal-W medium until their $A_{600\,nm}$ = 2–3. Cells were harvested and resuspended in 100 μl of 0.2 M NaOH. After 5 min at room temperature and a rapid centrifugation, the pellet was resuspended in 10 mM Tris-HCl, pH 6.8, 5% glycerol, 2% SDS, 4% β-mercaptoethanol, and 0.0025% bromophenol blue. It was boiled for 3 min and 6 μl of the supernatant was loaded on a 12.5% SDS-PAGE gel. Tubulin was detected after transfer onto a nitrocellulose membrane with an anti-tubulin antibody (1/2000) kindly provided by A. Baines (28).

Isolation of Mitochondria, Kinetic Measurements, Cytochrome Contents, Ancp Immunodetection, and EMA Labeling—Yeast cells used for isolation of mitochondria were grown in SGal-W to allow the plasmid to be maintained in transformants. The protocols and materials used to perform isolation of mitochondria, ADP/ATP transport, [^{3}H]ATR binding experiments, cytochrome content measurements, and protein immunostaining are described in De Marcos *et al.* (26). For determination of the relative ScAnc2p content mitochondria were isolated from cells grown in SGal-W. Different amounts of mitochondrial proteins were subjected to SDS-PAGE and transferred onto a nitrocellulose membrane that was then immunostained with an antibody raised against yeast porin (1/14,000) plus an antibody raised against the last 14 amino acids of ScAnc2p (1/7,000). After ECL detection with a GeneGnome system (Syngene, Ozyme), intensities of the signals were quantified with ImageJ (Rasband, W. S., National Institutes of Health). The ScAnc2p/porin ratio in arbitrary units was set at 1 for the wild-type protein.

The time course of CATR-induced release of bound N-ADP was studied by incubating freshly isolated mitochondria (0.5 mg of mitochondrial proteins/ml) at 16 °C in 2 ml of 120 mM KCl, 10 mM MOPS, pH 6.8, and 1 mM EDTA. Fluorescence measurements were performed as described in David *et al.* (12). EMA labeling of membrane-embedded ScAnc2p variants was performed on isolated mitochondria as described in David *et al.* (12).

In Vitro Synthesis of Precursor Proteins and Import into Yeast Mitochondria—The DNA fragments carrying the leucine variant ORF (EcoRI-BamHI) were subcloned into the pGEM4Z plasmid (kindly provided by M. Donzeau) for *in vitro* transcription by SP6 polymerase (TEBU, Ampliscribe). Precursor proteins were then synthesized in a rabbit reticulocyte lysate (Promega) in the presence of [^{35}S]methionine. Import reactions were performed as described in Ref. 26. The samples were subjected to a 15% SDS-PAGE and the labeled proteins were visualized with the Fluorescent Image Analyzer Fujifilm FLA-500. Radioactivity of the bands was quantified using the ImageJ software.

Respiratory Rates—Respiratory rates were measured with a Clark electrode in a 1-ml cell, thermostated at 30 °C. Freshly isolated mitochondria are diluted (0.1–0.3 mg/ml) in 5 mM KCl, 0.6 M mannitol, 10 mM MOPS, pH 6.8, 10 mM potassium P_i, pH 6.8, and 4 mM $MgCl_2$. State 3 and 4 respiration rates are determined in presence of NADH (0.5–2 mM), with or without ADP (100 μM) or with FCCP (1 μM).

Fluorescence Microscopy—To observe the mitochondrial network, the various yeast strains were transformed with a plasmid encoding a mutant GFP (S65T), which is targeted to mitochondria, pVT100U-mtGFP (29), a kind gift of W. Neupert and B. Westermann. Cells were then cultivated in 25 ml of a selective medium until $A_{600\,nm}$ = 2–4. The cell suspension (2 μl)

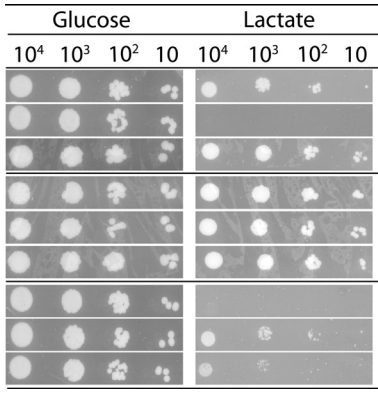

Ancp variant	Doubling time[a]	Growth yield[b]
Wild type	2h30	12
none	-	-
Ser147Pro	2h30	11
Pro43Ala	4h20	10
Ser147Ala	3h50	10
Pro247Ala	4h20	12
Pro43Leu	8-10h	5
Ser147Leu	5h	9
Pro247Leu	6h	10

FIGURE 2. **Leucine in place of proline is more deleterious to yeast growth than alanine.** *JL1Δ2Δ3u*$^-$ was transformed with the pRS314 plasmid containing no insert (no Ancp) or the indicated ScAnc2p variant encoding gene. Transformants were cultivated at 28 °C for 2 days on SC-W minimum medium (*Glucose*) or 4 days on lactate-containing rich medium (*Lactate*). $A_{600\ nm}$ was measured every 4 h during 80–300 h in lactate-rich liquid media to determine doubling time (hours) and growth yield ($A_{600\ nm}$ at the stationary phase of the cultures).

was mounted on a microscope slide under a coverslip. GFP was visualized by epifluorescence microscopy (Leica Microsystems DM-LB) under an oil immersion objective. The images were acquired with a SIS camera and processed with Corel Draw 9.0 suite software.

RESULTS

A Prolyl Residue Can Substitute for Transmembrane Ser-147—Ser-147 in TMH3 of ScAnc2p was mutated into proline to mimic what could be an evolutionary process, as suggested by Ancp sequence alignment (30). Indeed, in the second MCF signature motif P*X*(D/E)*XX*(K/R), the first residue is a proline in Ancp sequences from animals and it corresponds to a serine in trypanosoma, leishmania, plants, and fungi. The mutated ScAnc2p, S147P, was introduced into a yeast strain deleted for endogenous *ANC*, *JL1Δ2Δ3u*$^-$, of which growth on a non-fermentable carbon source such as lactate can be restored only by the presence of an active ScAnc2p. As can be seen in Fig. 2 (*third lane*), the S147P variant restored growth on lactate with characteristics (doubling time and growth yield) similar to that of the wild-type (WT) ScAnc2p. The empty plasmid did not allow growth on lactate, although the transformed strain was viable on glucose, a fermentable carbon source, which does not require functional mitochondria (Fig. 2, *second lane*).

The S147P variant is active enough to complement the *anc* null mutation. Next, we estimated the ScAnc2p contents in mitochondria from immunostaining experiments. The relative ScAnc2p content was determined after immunostaining of mitochondrial proteins. Mitochondria were isolated from cells grown in SGal-W. Different amounts of mitochondrial proteins were subjected to SDS-PAGE. After transfer, the nitrocellulose membrane was then immunodecorated with an antibody raised against ScAnc2p (31) plus an antibody raised against yeast porin (32). Intensities of the signals were quantified and the ScAnc2p/porin ratio in arbitrary units was set at 1 for the wild-type protein. The amount of the S147P variant represented more than 80% of the WT protein (Table 1), indicating the S147P mutation did not prevent ScAnc2p insertion into mitochondria.

This variant was further characterized at a molecular level, by measuring the ADP/ATP exchange parameters on isolated

TABLE 1
Mitochondrial ScAnc2p content and ADP/ATP exchange kinetic parameters on isolated mitochondria

ScAnc2p variant	Growth on lactate[a]	Relative ScAnc2p content[b]	$K_{m(ADP)}$[c]	V_{max}/K_m[c]
			μM	
WT	+	1	1.5 ± 0.2	58 ± 4
S147P	+	0.84 ± 0.10	0.44 ± 0.07	84.1 ± 0.9
P43A	+	0.92 ± 0.09	3.5 ± 0.3	17.7 ± 0.3
S147A	+	0.8 ± 0.01	3.1 ± 0.2	23.2 ± 1.2
P247A	+	0.66 ± 0.13	4.2 ± 0.4	11.2 ± 0.8
P43L	−	0.78 ± 0.07	10 ± 2	2 ± 0.2
S147L[b]	<	0.52 ± 0.06	7 ± 1	7.1 ± 0.5
P247L	≪	0.31 ± 0.09	25 ± 3	3.6 ± 0.3

[a] + and − indicate growth or absence of growth on lactate, respectively. < and ≪ indicate poor and very poor growth on lactate, respectively.
[b] The relative ScAnc2p content was determined after immunostaining of mitochondrial proteins with an antibody raised against yeast porin and an antibody raised against the last 14 amino acids of ScAnc2p. The ScAnc2p/porin ratio in arbitrary units was set at 1 for the wild-type protein. Data are the means of at least 2 experiments.
[c] Freshly isolated mitochondria were incubated in the presence of an energy generating system, an ATP detection enzymatic system based on NADP reduction, and variable concentrations of free ADP. The ADP/ATP exchange was followed at 340 nm. The given values are the means of three to six different experiments.

mitochondria. As presented in Table 1, the K_m value for external ADP is decreased 3.4 times and, the V_{max}/K_m ratio increased 1.4 times, indicating a higher efficiency at low nucleotide concentrations, compensating for a small decrease in Ancp content, as measured by immunostaining (Table 1). Overall, these results can account for similar growth properties of the two strains in lactate-rich medium, although at the molecular level a prolyl residue in place of Ser-147 modifies to some extent the kinetic properties of the exchange, probably because the local environment around position 147 does not fit exactly the larger steric hindrance of proline, which occurred later during the evolution of Ancp (Fig. 1).

Replacements of Transmembrane Pro-43, Ser-147, and Pro-247 with Alanine Do Not Prevent Ancp Activity—Proline residues are often present within TMH of membrane proteins and are known to induce a significant distortion named Pro-kink (33). The extent of the bending varies upon the position of the proline residue (34). This kink may play an important role in protein function by affording plasticity in the TMH (see for examples, Refs. 35 and 36).

As shown in Fig. 2, replacements of prolines/serine with alanine allowed growth restoration of the *JL1Δ2Δ3u*$^-$ strain on

TABLE 2
[^{3}H]ATR binding parameters

ScAnc2p variant	$B_{max(ATR)}$ [a]	$K_{D(ATR)}$ [a]	ATR-binding Ancp	$k_{cat} = V_{max}/B_{max}$ [b]	k_{cat}/K_m [b]
	pmol/mg	*nM*	*%*	*min^{-1}*	
WT	1010 ± 77	192 ± 25	100	86 ± 2	57 ± 9
P43A	380 ± 7	164 ± 6	41 ± 6	163 ± 5	47 ± 3
S147A	479 ± 23	133 ± 13	52 ± 6	150 ± 5	48 ± 5
P247A	211 ± 43	535 ± 202	34 ± 1	223 ± 41	53 ± 15
P43L	64 ± 5	173 ± 31	8 ± 1	313 ± 7	31 ± 6
S147L	55 ± 4	264 ± 38	10 ± 1	909 ± 48	130 ± 18
P247L	88 ± 10	378 ± 93	28 ± 7	1034 ± 83	41 ± 2

[a] Various [^{3}H]ATR concentrations were incubated with isolated mitochondria (1 mg). After incubation on ice (45 min), radioactivity associated to the pellet was counted to calculate the amount of [^{3}H]ATR bound to mitochondria. Nonspecific binding was measured in the presence of 500 μM CATR. The given values are the means of at least three different experiments.
[b] The V_{max}/B_{max} and k_{cat}/K_m ratios were calculated with data from Tables 1 and 2.

lactate, although the doubling times of the variant strains were increased as compared with the WT strain (Fig. 2). The ScAnc2p variant contents in mitochondria were reduced but not dramatically (66–92%, Table 1). However, these results were not in line with the amounts of ScAnc2p measured through [^{3}H]ATR binding experiments (Table 2). Indeed, the $B_{max(ATR)}$ values for the alanine variants were reduced 2–5 times when compared with that of the WT ScAnc2p. Immunostaining indicates the whole amount of ScAnc2p relative to porin, whereas [^{3}H]ATR binding experiments measure the amount of presumably properly folded ScAnc2p in mitochondria. Indeed, ATR binds to an Ancp conformation involved in the nucleotide exchange. The observed differences mean that only part of the variant carriers embedded in mitochondria are able to bind ATR, therefore presumably properly folded. The less properly folded variant is P247A because only 34% of the protein can bind ATR (Table 2). Besides, the $K_{D(ATR)}$ value is slightly decreased for P43A and S147A compared with that of the WT (1.2–1.4 times), whereas it is increased 2.8 times for the P247A variant (Table 2), indicating its folding is not optimal. These results could correlate with a decrease in nucleotide transport because ATR binding stabilizes Ancp in a conformation involved in transport and a partial overlapping of ATR and nucleotide binding sites has been suggested (37).

Therefore, we measured the ADP exchange kinetic properties of the variants on isolated mitochondria (Table 1). The $K_{m(ADP)}$ values were increased 2–2.8 times (Table 1). The change in the ATR affinity for the P247A variant correlates with a decrease of nucleotide binding, as estimated through the $K_{m(ADP)}$ value (2.8 times increase), which reflects productive nucleotide binding.

k_{cat} values can be calculated from the ratio of the V_{max} to the $B_{max(ATR)}$ values, if we consider that only the Ancp fraction able to bind ATR is active. As can be seen, the k_{cat} values are higher for alanine variants than for the wild-type (1.7–2.6 times, Table 2). Thus, although the mitochondrial amount of potentially active carrier is decreased, this is compensated for by an increase in the molecular specificity, k_{cat}/K_m, of the alanine variants (Table 1), resulting in an activity similar to that of the wild-type at low nucleotide concentrations. These results could be explained by the relatively small size of the alanine residue, which would not disturb interactions between the amino acids surrounding the existing prolines, thus preserving the local environment of the nucleotide-binding site, and probably the local distortion initially induced by the Pro/Ser-kink.

Replacements of Pro-43, Ser-147, and Pro-247 with Leucine Are More Deleterious to Yeast Growth Than with Alanine—Replacing Pro-43, Ser-147, and Pro-247 with leucines was more deleterious to yeast growth on lactate (Fig. 2), the most dramatic change being for the P43L variant, in which the doubling time was increased 4 times and growth yield decreased around 2.4 times. The relative ScAnc2p contents compared with the WT were 78 ± 7, 52 ± 6, and 31 ± 9% for the P43L, S147L, and P247L variants, respectively (Table 1). There was no correlation with the growth properties because the poorest growth was observed for the variant with the less decreased amount of ScAnc2p (P43L). We therefore estimated the maximum number of [^{3}H]ATR binding sites (Table 2). They were dramatically reduced representing only 5–9% of the WT (Table 2). Therefore, only a minor fraction of the variants embedded in the MIM could bind ATR (8, 10, and 28%), in correlation with the altered growth properties of the variant strains (Fig. 2). However, the $K_{D(ATR)}$ value was modified only for P247L, with a 3.5 times increase.

In Vitro Import of the Leucine Variants into Mitochondria Is Defective—The low levels of some leucine variant proteins in the MIM could arise from a defect of their import into mitochondria or of their stability once they are embedded in the MIM. We addressed this issue by studying *in vitro* WT ScAnc2p and leucine variant import into isolated yeast mitochondria. The corresponding genes were inserted in the pGEM4Z plasmid for their *in vitro* transcription and translation (see "Experimental Procedures"). All of the ScAnc2p carriers incubated with energized yeast mitochondria were partially resistant to PK digestion (Fig. 3*A*, *lanes 1* and *2*), thus partially imported into mitochondria. After PK treatment of energized mitoplasts, the part of the precursors protected from PK treatment was smaller for the variants than for the WT: 25% (P43L), 14% (S147L), and 15% (P247L) to be compared with 48% for the WT (Fig. 3, *A*, *lane 3*, and *B*). With de-energized mitochondria, ScAnc2p carriers were not fully protected from PK treatment (Fig. 3*A*, *lane 5*) indicating that the $\Delta\psi$ requirement for the leucine variant import followed the one for ScAnc2p. Evidently, the variants are less efficiently imported into W303 mitochondria than the WT ScAnc2p (30–50% of the WT, Fig. 3*B*), and this import defect may be even more pronounced *in vivo* in the leucine variant mitochondria.

Mitochondrial Cytochrome Contents Are Altered in Leucine Variants—Cell mitochondria content can be estimated from a measure of the cell ScAnc2p and cytochrome contents. Cell ScAnc2p contents were estimated from immunostaining of whole cell extract proteins with antibodies raised against ScAnc2p and tubulin (38), a cytosolic protein, and expressed as the ratios of ScAnc2p/tubulin. The cellular ScAnc2p content decreased for the leucine variants as it represented 80 ± 3% (P43L), 59 ± 14% (S147L), and 41 ± 2% (P247L) of the WT content (data not shown). Therefore, cytochrome contents of isolated mitochondria and whole cells were measured for comparison with the ScAnc2p contents (Fig. 4*A*). There was an increase in the mitochondrial cytochrome cc_1 content for all the variants, the largest one being observed for P43L. However,

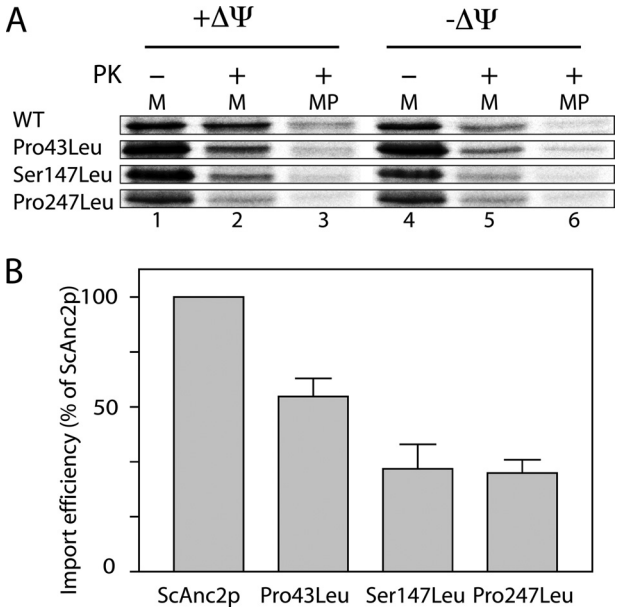

FIGURE 3. ***In vitro* import of the leucine variants into isolated yeast mitochondria.** *A,* [^{35}S]methionine-labeled precursors were incubated with isolated yeast mitochondria, either energized (+ΔΨ) or deenergized (−ΔΨ), for 30 min at 25 °C. Mitochondria (*lanes 1*, *2*, *4,* and *6*) or mitoplasts (MP, *lanes 3* and *6*) were then treated with proteinase K (*PK*, 100 μg/ml; *lanes 2*, *3*, *5*, and *6*) for 5 min at 4 °C. They were further isolated by centrifugation, washed, and resuspended in sample buffer before SDS-PAGE. *Lane 1* corresponds to 10% of the amount of radiolabeled precursor added to each import assay. *B,* import efficiency for the leucine variants relative to the WT (ScAnc2p in mitoplast after PK digestion/ScAnc2p before the import reaction).

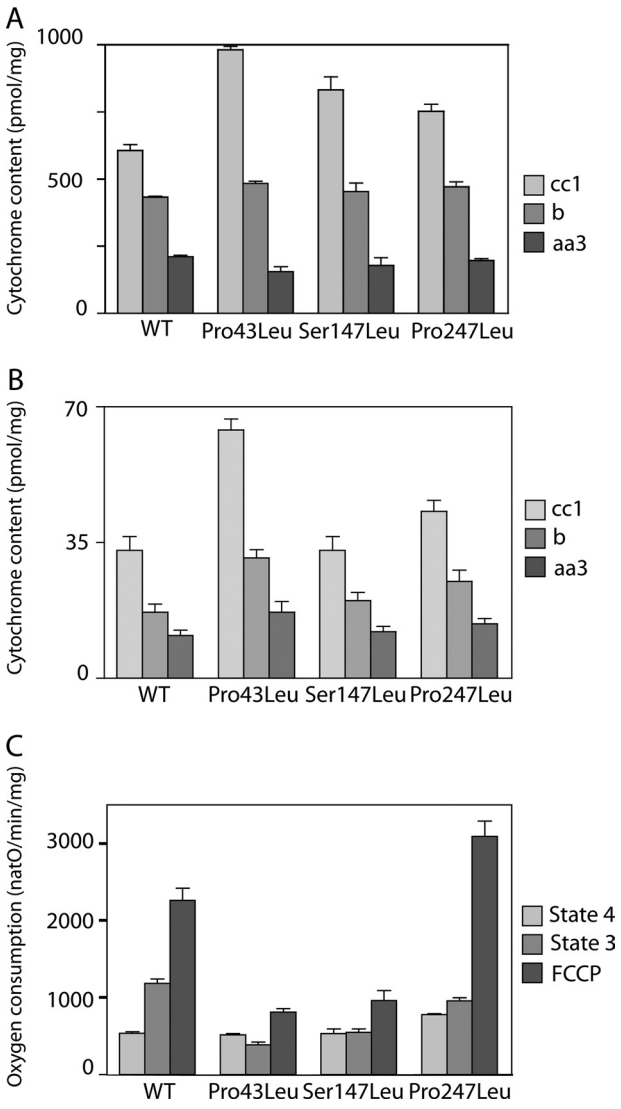

FIGURE 4. **Mitochondria (*A*) and cell (*B*) cytochrome contents and mitochondrial respiration rate (*C*) of the leucine variants.** The cytochrome contents are expressed in picomole/mg of proteins (*A*) or picomole/mg dry weight (*B*). Oxygen consumption (natO/min/mg) was measured in the presence of NADH (0.2–5 mM) without (state 4) or with 100 μM ADP (state 3). Maximal rate was measured in the presence of 1 μM FCCP.

with respect to the cytochrome aa_3 and *b* contents, it was roughly similar to that of the WT, whatever the variant, suggesting an altered overall composition of the cytochromes in the MIM. At the cellular level, there was a strong increase in the whole cytochrome content for P43L, to a lesser extent for P247L, but none for S147L (Fig. 4*B*). If we consider only the cytochrome aa_3 content, which is membranous, we can propose that the amount of mitochondria per cell remained similar (S147L) or was slightly increased (P43L and P247L), whereas the mitochondrial cytochrome contents were significantly modified, leading to a 10–25 times decrease in the ScAnc2p/cytochrome ratio. This was an indication of important changes in the MIM protein composition induced by mutations into leucine of Pro-43, Ser-147, or Pro-247 of ScAnc2p.

Mitochondrial Oxygen Consumptions—Cytochrome content alteration may result in modified respiration. Oxygen consumption was measured for mitochondria isolated from cells grown in SGal-W (Fig. 4*C*). The state 4 rate is comparable with the WT for P43L and S147L, and is 1.4 times higher for P247L, probably due to a higher proton permeability of the inner mitochondrial membrane. It is barely stimulated by ADP, in line with the impaired nucleotide exchange properties observed for the leucine variants (Table 1). The uncoupler FCCP increased to some extent state 3 respiration rates (Fig. 4*C*). For P43L and S147L variants, the uncoupler FCCP led to a lower increase in oxygen consumption than for WT. This is not related to a global cytochrome content decrease but in line with a slower turnover of cytochrome *c* oxidase (data not shown). On the contrary, the P247L variant displays a very high respiration rate in the presence of FCCP in line with a higher turnover of cytochrome *c* oxidase (data not shown).

Mitochondria and Cell Morphologies Are Altered in Leucine Variants—As a consequence, we addressed the question of the mitochondrial morphology in the leucine variant strains. Those were transformed with a plasmid encoding a mitochondria-targeted GFP under the control of the constitutive *ADH* promoter, pVT100U-mtGFP (29). Cells were observed during the exponential phase by epifluorescence microscopy. Results were compared between WT ScAnc2p, the alanine variants, and the leucine variants (Fig. 5). A clear filamentous mitochondrial network is observed in the WT and alanine variant strains, whereas in the leucine variants, it appears highly fragmented/punctuated, indicating that the mitochondrial fission and fusion processes are unbalanced in these mutants. The percent of fragmented/punctuated network was estimated for each strain. The most dramatic effects were observed for the P43L and P247L

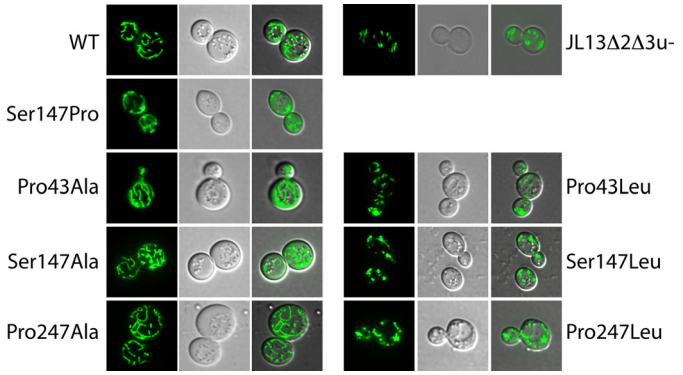

FIGURE 5. **The mitochondrial morphology is modified in the leucine variant cells.** Cells expressing the wild-type or the variants were transformed with a plasmid encoding GFP (S65T) targeted to mitochondria to visualize the mitochondrial network. Cells were cultivated in a selective galactose-containing medium until $A_{600\ nm}$ reached a value of 2–4. GFP was visualized with an epifluorescence microscope (Leica Microsystems DM-LB) under an oil immersion objective. *WT* stands for wild type ScAnc2p.

TABLE 3
Mitochondrial network observed by epifluorescence and transmission electron microscopies

ScAnc2p variant	Growth on lactate	Disrupted mitochondrial network[a]	Number of mitochondria per cell[b]
		%	
WT	+	15 ± 9	2.5 ± 1.5
None[c]	−	72 ± 13	4.1 ± 1.8
S147P	+	11 ± 2	2.8 ± 1.7
P43A	+	14 ± 2	3.3 ± 2.3
S147A	+	12 ± 6	3.2 ± 1.9
P247A	+	9 ± 8	2.7 ± 1.9
P43L	−	75 ± 3	4.1 ± 2.9
S147L	<	55 ± 19	3.7 ± 2.2
P247L	≪	71 ± 12	3.5 ± 2.0

[a] Yeast cells were transformed with the pVT100U-mtGFP plasmid. Cells were harvested during the log phase and observed by epifluorescence microscopy (Fig. 5). The mitochondrial network was classified into two types: filamentous/intermediate and disrupted (fragmented and punctuated). The percent of cells exhibiting a disrupted network was estimated from the observation of at least 240 fluorescent cells per variant strain.

[b] Cells were grown in 100 ml of SGal-W until $A_{600\ nm} = 3$. Harvested cells were placed on the surface of Formvar-coated copper grids (400 mesh). Each loop was quickly submersed in liquid propane (−180 °C) and then transferred to a precooled solution of 4% osmium tetroxide in dry acetone at −82 °C for 72 h for substitution/fixation. Samples were gradually warmed to room temperature, and washed in dry acetone. Specimens were stained for 1 h with 1% uranyl acetate in acetone at 4 °C, rinsed, and infiltrated with Araldite (epoxy resin, Fluka). Ultrathin sections (70 nm) were stained with lead citrate. Observations were performed on a Hitachi H7650 (120 kV) electron microscope in high contrast mode and equipped with ORIUS SC1000 11 Mpx camera (GATAN). Images were analyzed with the acquisition software Digital Micrograph (GATAN). The number of mitochondria per cell was counted for at least 50 cells per variant strain.

[c] Corresponding to the *JL13Δ2Δ3u*$^-$ strain.

variants for which the percent of filamentous mitochondria fell to less than 30%, as can be observed for the strain devoid of Ancp, *JL1Δ2Δ3u*$^-$ (Table 3). This indicates that the network disruption is linked to an important alteration of the ADP/ATP carrier activity, which leads to a modification of the fission/fusion balance in these mutants.

Cell morphology of the leucine variants observed under electron microscopy was closer to that of cells deleted for its endogenous *ANC* genes (*JL1Δ2Δ3u*$^-$) than to that of WT cells or of the parental strain *W303* (data not shown). Furthermore, their mitochondria number increased 1.4–1.6 times, in line with a more fragmented mitochondrial network, whereas it was similar to that of the WT for the alanine variants (Table 3).

Kinetic Parameters Account for Poor ADP/ATP Exchange Activities of Leucine Variants on Isolated Mitochondria—Replacement of Pro-43, Ser-147, and Pro-247 of ScAnc2p with leucine is detrimental to cell growth, mitochondrial morphology, ScAnc2p folding, and probably to the ADP/ATP exchange activity too. It was measured on isolated mitochondria (Table 1) as described under "Experimental Procedures." The Michaelis constant was increased 6–17 times, indicating that the productive ADP binding was disrupted for the leucine variants. If we refer the V_{max} value to that of the maximum number of [^{3}H]ATR binding sites, the molecular activity (k_{cat}) of the leucine variants is highly increased (Table 2), which is quite surprising. On the other hand, the k_{cat}/K_m ratio, or specificity constant, is highly increased for the S147lL, whereas it is decreased for the P43L variant, indicating that the productive nucleotide binding may be modified for those variants. Last, if we consider the V_{max}/K_m ratio, which reflects the mitochondrial efficiency of the exchange, it is much more decreased for the leucine variants than what was observed for the alanine variants (Table 1). Therefore, the mitochondrial effectiveness is so low that the leucine variant strains barely grow on lactate.

A poor ADP/ATP exchange activity can be accounted for either by a poor substrate binding or by disturbed carrier conformational changes necessary to the nucleotide transport. We first investigated ADP binding through the use of N-ADP. N-ADP is a non-transportable fluorescent ADP analog whose binding properties to Ancp can be examined with isolated mitochondria (39). The $K_{½}$ value of N-ADP binding to the yeast ScAnc2p is 1.7 μM (12). N-ADP binding could be measured only with the S147L variant. The $K_{½}$ value was 2.4 ± 1.4 μM, close to that of the WT. Therefore, we confirmed this variant can still bind ADP although its exchange activity is low. No N-ADP binding could be measured for the two other variants. Indeed, no fluorescence increase was observed after CATR addition. This could be due to absence of either N-ADP binding or CATR-induced N-ADP displacement.

EMA Labeling Suggests That S147L Mutation Prevents Stabilization of ScAnc2p-CATR Complex—Nucleotide transport is associated with conformational changes involving movements of the matrix loops. The V176C mutation in the middle of the matrix loop m2 (Fig. 6*A*) is a convenient tool to report these conformational changes (12). Indeed, in the absence or presence of ADP or BA, EMA labels V176C of a cysteine-less ScAnc2p variant (Anc2CLp^{V176C}). In contrast, CATR prevents EMA labeling, suggesting that large conformational changes of matrix loop m2 may take place upon ligand binding. The P43L, S147L, and P247L mutations were introduced into Anc2CLp^{V176C}. EMA labeling was performed with frozen-thawed mitochondria in the absence or presence of CATR or BA or ADP (Fig. 6*B*). As can be seen, these variants were always labeled with EMA, whatever the added ligand, whereas Anc2CLp^{V176C} was labeled in the presence of BA but not of CATR (see Ref. 12 and Fig. 6*B*). CATR concentration was increased 10–100 times without preventing EMA labeling of the leucine variants. These results suggest that these mutations could preclude either CATR binding or some of the conformational changes essential for ADP/ATP transport. Noteworthy, the B_{max} value of [^{3}H]ATR binding is low for the three leucine variants (Table 2) in favor of a poor CATR binding. This could

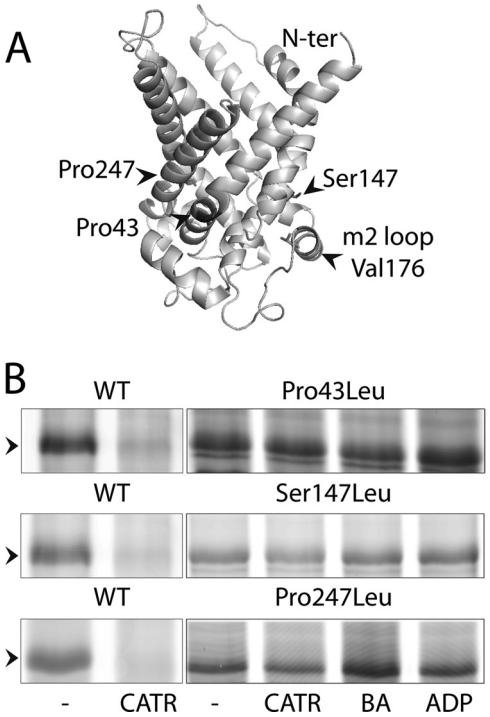

FIGURE 6. *A,* the three-dimensional structure of ScAnc2p was modeled as described in David *et al.* (12). *B,* EMA labeling of V176C in the leucine variants. Mitochondria were isolated from ScAnc2p^{V176C} non-mutated (*WT*) or mutated (P43L, S147L, and P247L). Frozen-thawed mitochondria were incubated (8 mg of proteins/ml) with no ligand (none) or with 20 μM CATR or 20 μM BA or 20 μM ADP for 15 min on ice. EMA labeling (200 μM) was performed for 30 min on ice in the dark. The reaction was stopped with 20 mM DTT. Samples were subjected to SDS-PAGE and fluorescence was visualized at 532 nm. The position of ScAnc2CLp^{V176C}, indicated by an *arrow*, was controlled by immunoblotting after transfer of the gel onto a nitrocellulose membrane.

explain why V176C is always labeled even in the presence of CATR. However, in the case of S147L, CATR could displace bound N-ADP (see above). Therefore, this mutant can bind CATR but would be unable to perform the conformational changes necessary to stabilize the carrier-CATR complex, thus allowing EMA labeling of V176C even in the presence of the inhibitor.

DISCUSSION

Proline in α helices causes a kink because its amide hydrogen is unable to complete the normal H-bonding chain of the helix, and steric or rotamer effects prevent proline from adapting the preferred helical geometry. Proline-kinked helices appear to be a relatively common structural element in transmembrane proteins (33). From a structural point of view, Pro-kinks provide an easy way to introduce a curvature in a TMH. In the case of the BfAnc1p three-dimensional structure, the presence of 3 Pro-kinked helices out of 6 creates a cavity open to the IMS. A similar feature is observed in the recently solved three-dimensional structure of the rat UCP2 that belongs to the MCF (41).

The functional role of Pro-kinks remains elusive despite mutagenesis studies with several membrane proteins. Pro-kinks destabilize the hydrogen bond network that normally stabilizes the secondary structure. Their functional role was approached by molecular dynamics experiments, in particular in the case of BfAnc1p (13). In these studies, ADP was forced to enter deeply into BfAnc1p by two independent biased simulations on a very short 20-ns time scale. Yet, ADP binding can induce radial outward displacements toward the membrane of the odd-numbered TMH provoking a drastic rearrangement of the salt bridges that initially closed the cavity on the matrix side. This reorganization unlocks the three odd-numbered TMH allowing the protein to expand in the matrix half. Besides, deuterium exchange experiments carried out with the BfAnc1p showed that TMH1, -2, -3, and -5 were much less exposed to the solvent on the IMS side in the BA complex than in the CATR complex, indicating rearrangement of the two halves of the carrier: the one oriented through the matrix and the other one to the IMS, one relative to the other (14). Similar experiments carried out with yeast ScAnc2p evidenced inhibitor-dependent deuterium accessibility: the matrix loops were more deuterated in the presence of BA than in the presence of CATR (40). The largest differences in the deuteration levels were exhibited by the regions encompassing the MCF signature motifs located at the bottom of the cavity, underlining a potential hinge role of the transmembrane prolines belonging to these motifs.

In the CATR conformation, Ancp is open to the intermembrane space and locked on the matrix side by twisting the C-terminal regions of the odd-numbered TMH. The small soluble α helices in the matrix loops reinforce this plug. However, this side of the carrier has to be open for Ancp to operate substrate transport. In the recently solved solution structure of UCP2 (41), a small aperture is described on the matrix side resulting mainly from a relative displacement of the small amphipatic helix h56 in the middle of the m3 matrix loop. Besides, TMH5 has shifted between TMH4 and TMH6, breaking the pseudo 3-fold symmetry in UCP2. Pro-232 in TMH5 is therefore closer to the IMS than Pro-33 and Pro-136 of TMH1 and TMH3, respectively. These observations could give a clue as to how movements around the three conserved prolines open the cavity on the matrix side (41).

To get insights into the role of these three prolines in Ancp, we mutated the proline/serine residues of the MCF signature sequence of ScAnc2p into alanine or leucine. Mutation into alanine was not deleterious to Ancp activity at the cell and mitochondrial levels. Alanine can induce a small distortion in a TMH, but not as big as proline. Its small size probably does not induce perturbations of the local environment in its vicinity. This could explain why replacement of Pro/Ser with alanine did not impair ScAnc2p activity. However, a closer examination of the results evidence that these mutations affected the mitochondrial ScAnc2p content and ATR binding properties. These results are in favor of a role of the three prolines in ScAnc2p biogenesis in mitochondria and in binding of ATR, and maybe nucleotide. Their mutation could impair in one way or another the conformational changes normally arising from ligand binding.

A deeper insight into the role of prolines/serine residues was obtained by their mutation into leucine. They dramatically affected yeast growth and morphology, mitochondrial function and protein content, and ADP/ATP exchange activity to an extent depending on the position of the mutated residue. Evi-

dently, the three residues do not have similar roles, although all are involved in the above-mentioned functions.

ScAnc2p variant mitochondrial levels do not correlate when the amounts of ScAnc2p were determined from immunostaining or [^{3}H]ATR binding experiments (Table 2). Immunostaining detects even partially imported ScAnc2p, which *in vitro* can be accessible to PK when the outer membrane is disrupted (mitoplast), and therefore not taken into account for calculation of import efficiency. Comparison of [^{3}H]ATR binding and *in vitro* import experiments reinforces the hypothesis of the variant carriers being present in mitochondria in two different populations: one more or less misfolded and unable to bind ATR, the other one properly folded and competent for ATR binding. Indeed, conformational changes studied by EMA labeling appeared to be hindered in the case of the leucine variants, which are always labeled, whatever the ligand. These variants would be unable to adopt or to be stabilized in a CATR-like conformation, and would preferably adopt a BA-like conformation. This hypothesis could not be evaluated more in depth mainly because of the poor yield of mitochondria isolated from the leucine variants due to severe functional alterations, precluding BA binding measurements or carrier purification to carry out intrinsic fluorescence measurements, similar to those described for the WT (42).

P43L mutation resulted in altered ATR binding properties. Although the ScAnc2p amount reached 80% of the WT, only 8% of the carrier embedded in mitochondria could bind ATR. This could mean that the majority of the variant carrier is not properly imported and/or folded. *In vitro* import experiments evidenced lower import efficiency with wild-type mitochondria, which could be even lower *in vivo* with mitochondria expressing the P43L variant. Indeed, in this case the mitochondrial energization state would not be sufficient to allow efficient protein import. However, this import defect is not a general one as it does not apply to the cytochromes and even the reverse is true for cytochrome *c*, which location is the IMS, whereas that of cytochromes aa_3 and *b* is the MIM. In addition, this does not correlate with an increase in the respiratory function.

Noteworthy, cell morphology of the leucine variants as seen with electron microscopy is typical of defective mitochondrial oxidative phosphorylation. This is also the case of *JL1*Δ*2*Δ*3u*$^-$, the *ANC* disrupted strain used in this study. The consequences are a highly fragmented/punctuated mitochondrial network (75%) and a significant increase in the number of mitochondria per cell for the P43L variant. At the molecular level, the high turnover number applies to a minor fraction of the carrier and, consequently does not reflect adequately the properties of the P43L mitochondria. The major population of this variant does not bind CATR (as indicated by [^{3}H]ATR binding experiments, Table 2) and therefore cannot be stabilized in a CATR-like conformation (EMA labeling, Fig. 6*B*). However, Ancp conformational changes are essential to nucleotide translocation. This variant would be unable to adopt a CATR-like conformation necessary to achieve nucleotide transport (see above). Furthermore, when carrying N-ADP binding experiments, we observed that after adding N-ADP to mitochondria, the fluorescence level remained very high, contrary to what is usually observed with the WT. Because only the soluble form of N-ADP is fluorescent, this indicates that P43L poorly binds N-ADP. This is consistent with the high $K_{m(\mathrm{ADP})}$ values determined from exchange experiments.

As a conclusion, Pro-43 is involved in ADP and ATR/CATR binding, and we can suggest that mutating this residue into leucine prevents conformational changes induced by ligand binding, inhibitors, and substrates. This sustains a role of Pro-43 as a hinge, as formerly proposed by Pebay-Peyroula *et al.* (1). This residue does not seem to be strongly involved in Ancp biogenesis although its mutation into leucine modifies dramatically the mitochondrial fusion/fission balance. This is the first time that a perturbation of the mitochondrial network is described as a consequence of an Ancp defect.

In the case of the P247L mutation, the mitochondrial ScAnc2p content was severely disabled, as well as ATR binding properties. Pro-247 is therefore highly involved in Ancp mitochondrial import, contrary to Pro-43, as seen from *in vitro* import experiments. A striking difference between Pro-43 and Pro-247 stands in the kinetic ADP/ATP exchange parameters. The $V_{\max}$ value for P247L is similar to that of the wild-type but the $K_{m(\mathrm{ADP})}$ value is highly increased, indicating perturbations in productive nucleotide binding. Pro-247 is located in the C-terminal part of TMH5, which displays the Ancp signature sequence, RRRMMM. This region of BfAnc1p exhibited similar accessibility to the solvent whatever the inhibitor bound (14), suggesting TMH5 is less flexible than its counterparts TMH1 and -3. This is in accordance with our results and with molecular dynamics experiments during which, movements around the prolyl residue in TMH5 are less important than movements around the prolyl residue in TMH1 (13). Nonetheless, the low level of nucleotide exchange, reflecting the low content of active carrier (see the low number of [^{3}H]ATR binding sites), was consistent with the fragmented mitochondrial network, similarly to what was observed for the P43L mutation.

The S147L mutation has less dramatic effects on the mitochondrial fission/fusion balance and this mutant can still bind N-ADP. Therefore its involvement is more in ATR/CATR binding. The conformational changes induced by nucleotide binding and stabilizing the nucleotide-Ancp complex are probably not mediated by movements around Ser-147. This residue is located in TMH3, which is directly linked to matrix loop m2, which was supposed to be the primary nucleotide binding site from the matrix space (43, 44). However, as can be drawn from exchange measurements, Ser-147 participates in the conformational changes necessary to translocation although less importantly than Pro-43.

In conclusion, replacement of the prolines/serine inducing kinks in TMH1, -3, and -5 with leucine, a large helix forming amino acid, permitted the exploration of their putative hinge role in the nucleotide transport mechanism. We confirmed this role because none of the leucine mutants can be stabilized in the CATR-like conformation. Interestingly, the three Pro/Ser residues cooperate to operate conformational changes because whatever the mutated position, each one prevents movements of matrix loop m2.

However, we also showed that the hinge role is modulated according to the position of proline within the sequence: Pro-43 is mainly involved in conformational changes induced by ligand

binding and Ser-147 in nucleotide translocation itself; in contrast Pro-247 seems to be less involved in these processes. However, Pro-247, along with Ser-147 but with a lesser degree, plays another critical role during Ancp biogenesis, *i.e.* import into the MIM, whereas Pro-43 contribution to this process is less significant. Because these prolines belong to the MCF sequence signatures, their involvement in the general mechanism of the mitochondrial carrier import is probably a rule for all MCF members. In addition, the three prolines/serines unexpectedly appear also to play a critical role in other aspects of mitochondrial biogenesis as their replacements with leucine result in alterations of both the morphology of mitochondrial network and assembly of the respiratory chains. This is likely to be related with the key role of Ancp in cell energetics.

Another kink is also observed in both BfAnc1p and UCP2 at the level of a conserved PTQA sequence in TMH2. It is located close to Arg-79 of BfAnc1p, which itself is perfectly conserved among Ancp, and which mutation into histidine inactivates ScAnc2p (*op1* mutation (45)). Arg-79 forms a salt bridge with the carboxylate of CATR not shared with ATR (47) Arg-79 is likely to act during nucleotide binding/transport, and therefore Pro-81 to play a role in conformational changes. This will be investigated by replacement with alanine and leucine.

Acknowledgment—We thank Bénédicte Salin (IBGC, UMR5095) for technical skills during transmission electron microscopy experiments.

REFERENCES

1. Pebay-Peyroula, E., Dahout-Gonzalez, C., Kahn, R., Trézéguet, V., Lauquin, G. J.-M., and Brandolin, G. (2003) Structure of mitochondrial ADP/ATP carrier in complex with carboxyatractyloside. *Nature* **426,** 39–44
2. Morozzo Della Rocca, B., Miniero, D. V., Tasco, G., Dolce, V., Falconi, M., Ludovico, A., Cappello, A. R., Sanchez, P., Stipani, I., Casadio, R., Desideri, A., and Palmieri, F. (2005) Substrate-induced conformational changes of the mitochondrial oxoglutarate carrier. A spectroscopic and molecular modelling study. *Mol. Membr. Biol.* **22,** 443–452
3. Tonazzi, A., Giangregorio, N., Palmieri, F., and Indiveri, C. (2005) Relationships of cysteine and lysine residues with the substrate binding site of the mitochondrial ornithine/citrulline carrier. An inhibition kinetic approach combined with the analysis of the homology structural model. *Biochim. Biophys. Acta* **1718,** 53–60
4. Kunji, E. R., and Robinson, A. J. (2006) The conserved substrate binding site of mitochondrial carriers. *Biochim. Biophys. Acta* **1757,** 1237–1248
5. Perchiniak, E., Lawrence, S. A., Kasten, S., Woodard, B. A., Taylor, S. M., and Moran, R. G. (2007) Probing the mechanism of the hamster mitochondrial folate transporter by mutagenesis and homology modeling. *Biochemistry* **46,** 1557–1567
6. De Lucas, J. R., Indiveri, C., Tonazzi, A., Perez, P., Giangregorio, N., Iacobazzi, V., and Palmieri, F. (2008) Functional characterization of residues within the carnitine/acylcarnitine translocase RX2PANAAXF distinct motif. *Mol. Membr. Biol.* **25,** 152–163
7. Walker, J. E., and Runswick, M. J. (1993) The mitochondrial transport protein superfamily. *J. Bioenerg. Biomembr.* **25,** 435–446
8. Nelson D. R., Felix C. M., and Swanson J. M. (1998) Highly conserved charge-pair networks in the mitochondrial carrier family. *J. Mol. Biol.* **277,** 285–308
9. Falconi, M., Chillemi, G., Di Marino, D., D'Annessa, I., Morozzo della Rocca, B., Palmieri, L., and Desideri, A. (2006) Structural dynamics of the mitochondrial ADP/ATP carrier revealed by molecular dynamics simulation studies. *Proteins* **65,** 681–691
10. Gray, T. M., and Matthews, B. W. (1984) Intrahelical hydrogen bonding of serine, threonine, and cysteine residues within α-helices and its relevance to membrane-bound proteins. *J. Mol. Biol.* **175,** 75–81
11. Ballesteros, J. A., Deupi, X., Olivella, M., Haaksma, E. E., and Pardo, L. (2000) Serine and threonine residues bend α-helices in the $\chi(1) = \gamma(-)$ conformation. *Biophys. J.* **79,** 2754–2760
12. David, C., Arnou, B., Sanchez, J. F., Pelosi, L., Brandolin, G., Lauquin, G. J.-M., and Trézéguet, V. (2008) Two residues of a conserved aromatic ladder of the mitochondrial ADP/ATP carrier are crucial to nucleotide transport. *Biochemistry* **47,** 13223–13231
13. Wang Y., and Tajkhorshid, E. (2008) Electrostatic funneling of substrate in mitochondrial inner membrane carriers. *Proc. Natl. Acad. Sci. U.S.A.* **105,** 9598–9603
14. Rey, M., Man, P., Clémençon, B., Trézéguet, V., Brandolin, G., Forest, E., and Pelosi, L. (2010) Conformational dynamics of the bovine mitochondrial ADP/ATP carrier isoform 1 revealed by hydrogen/deuterium exchange coupled to mass spectrometry. *J. Biol. Chem.* **285,** 34981–34990
15. Endres, M., Neupert, W., and Brunner, M. (1999) Transport of the ADP/ATP carrier of mitochondria from the TOM complex to the TIM22.54 complex. *EMBO J.* **18,** 3214–3221
16. Sirrenberg, C., Endres, M., Fölsch, H., Stuart, R. A., Neupert, W., and Brunner, M. (1998) Carrier protein import into mitochondria mediated by the intermembrane proteins Tim10/Mrs11 and Tim12/Mrs5. *Nature* **391,** 912–915
17. Zara, V., Ferramosca, A., Capobianco, L., Baltz, K. M., Randel, O., Rassow, J., Palmieri, F., and Papatheodorou, P. (2007) Biogenesis of yeast dicarboxylate carrier. The carrier signature facilitates translocation across the mitochondrial outer membrane. *J. Cell Sci.* **120,** 4099–4106
18. Brix, J., Rüdiger, S., Bukau, B., Schneider-Mergener, J., and Pfanner, N. (1999) Distribution of binding sequences for the mitochondrial import receptors Tom20, Tom22, and Tom70 in a presequence-carrying preprotein and a non-cleavable preprotein. *J. Biol. Chem.* **274,** 16522–16530
19. Vial, S., Lu H., Allen, S., Savory, P., Thornton, D., Sheehan, J., and Tokatlidis, K. (2002) Assembly of Tim9 and Tim10 into a functional chaperone. *J. Biol. Chem.* **277,** 36100–36108
20. Curran, S. P., Leuenberger, D., Oppliger, W., and Koehler, C. M. (2002) The Tim9p-Tim10p complex binds to the transmembrane domains of the ADP/ATP carrier. *EMBO J.* **21,** 942–953
21. Vasiljev, A., Ahting, U., Nargang, F. E., Go, N. E., Habib S. J., Kozany, C., Panneels, V., Sinning, I., Prokisch, H., Neupert, W., Nussberger, S., and Rapaport, D. (2004) Reconstituted TOM core complex and Tim9/Tim10 complex of mitochondria are sufficient for translocation of the ADP/ATP carrier across membranes. *Mol. Biol. Cell* **15,** 1445–1458
22. Cunningham, B. C., and Wells, J. A. (1989) High-resolution epitope mapping of hGH-receptor interactions by alanine-scanning mutagenesis. *Science* **244,** 1081–1085
23. Morrison, K. L., and Weiss, G. A. (2001) Combinatorial alanine scanning. *Curr. Opin. Chem. Biol.* **5,** 302–307
24. Eilers, M., Patel, A. B., Liu, W., and Smith, S. O. (2002) Comparison of helix interactions in membrane and soluble α-bundle proteins. *Biophys. J.* **82,** 2720–2736
25. Brandolin, G., Le Saux, A., Trézéguet, V., Vignais, P. V., and Lauquin, G. J.-M. (1993) Biochemical characterisation of the isolated Anc2 adenine nucleotide carrier from *Saccharomyces cerevisiae* mitochondria. *Biochem. Biophys. Res. Commun.* **192,** 143–150
26. De Marcos Lousa, C., Trézéguet, V., Dianoux, A. C., Brandolin, G., and Lauquin, G. J.-M. (2002) The human mitochondrial ADP/ATP carriers. Kinetic properties and biogenesis of wild-type and mutant proteins in the yeast *S. cerevisiae*. *Biochemistry* **41,** 14412–14420
27. Kushnirov, V. V. (2000) Rapid and reliable protein extraction from yeast. *Yeast* **16,** 857–860
28. Woods, A., Sherwin, T., Sasse, R., MacRae, T. H., Baines, A. J., and Gull, K. (1989) Definition of individual components within the cytoskeleton of *Trypanosoma brucei* by a library of monoclonal antibodies. *J. Cell Sci.* **93,** 491–500
29. Westermann, B., and Neupert, W. (2000) Mitochondria-targeted green fluorescent proteins. Convenient tools for the study of organelle biogenesis in *Saccharomyces cerevisiae*. *Yeast* **16,** 1421–1427
30. Nury, H., Dahout-Gonzalez, C., Trézéguet, V., Lauquin, G. J.-M., Brandolin, G., and Pebay-Peyroula, E. (2006) Relations between structure and

function of the mitochrondrial ADP/ATP carrier. *Annu. Rev. Biochem.* **75,** 713–741
31. Brandolin, G., Boulay, F., Dalbon, P., and Vignais, P. V. (1989) Orientation of the N-terminal region of the membrane-bound ADP/ATP carrier protein explored by antipeptide antibodies and an arginine-specific endoprotease. Evidence that the accessibility of the N-terminal residues depends on the conformational state of the carrier. *Biochemistry* **28,** 1093–1100
32. Michejda, J., Guo, X. J., and Lauquin, G. J.-M. (1990) The respiration of cells and mitochondria of porin-deficient yeast mutants is coupled. *Biochem. Biophys. Res. Commun.* **171,** 354–361
33. von Heijne, G. (1991) Proline kinks in transmembrane α-helices. *J. Mol. Biol.* **218,** 499–503
34. Thomas, R., Vostrikov, V. V., Greathouse, D. V., and Koeppe, R. E., 2nd (2009) Influence of proline upon the folding and geometry of the WALP19 transmembrane peptide. *Biochemistry* **48,** 11883–11891
35. Decaffmeyer, M., Shulga, Y. V., Dicu, A. O., Thomas, A., Truant, R., Topham, M. K., Brasseur, R., and Epand, R. M. (2008) Determination of the topology of the hydrophobic segment of mammalian diacylglycerol kinase ε in a cell membrane and its relationship to predictions from modeling. *J. Mol. Biol.* **383,** 797–809
36. Aoki, S., Thomas, A., Decaffmeyer, M., Brasseur, R., and Epand, R.M. (2010) The role of proline in the membrane re-entrant helix of caveolin-1. *J. Biol. Chem.* **285,** 33371–33380
37. Vignais, P. V., Duée, E. D., Vignais, P. M., and Huet, J. (1966) Effects of atractyligenin and its structural analogues on oxidative phosphorylation and on the translocation of adenine nucleotides in mitochondria. *Biochim. Biophys. Acta* **118,** 465–483
38. Solomon, F. (1991) Analyses of the cytoskeleton in *Saccharomyces cerevisiae*. *Annu. Rev. Cell Biol.* **7,** 633–662
39. Block, M. R., Lauquin, G. J.-M., and Vignais P. V. (1982) Interaction of 3′-*O*-(1-naphthoyl)adenosine 5′-diphosphate, a fluorescent adenosine 5′-diphosphate analogue, with the adenosine 5′-diphosphate/adenosine 5′-triphosphate carrier protein in the mitochondrial membrane. *Biochemistry* **21,** 5451–5457
40. Clémençon, B., Rey, M., Trézéguet, V., Forest, E., and Pelosi, L. (2011) Yeast ADP/ATP carrier isoform 2. Conformational dynamics and role of the RRRMMM signature sequence methionines. *J. Biol. Chem.* **286,** 36119–36131
41. Berardi, M. J., Shih, W. M., Harrison, S. C., and Chou, J. J. (2011) Mitochondrial uncoupling protein 2 structure determined by NMR molecular fragment searching. *Nature* **476,** 109–113
42. Roux, P., Le Saux, A., Trézéguet, V., Fiore, C., Schwimmer, C., Dianoux, A. C., Vignais, P. V., Lauquin, G. J.-M., and Brandolin, G. (1996) Conformational changes of the yeast mitochondrial adenosine diphosphate/adenosine triphosphate carrier studied through its intrinsic fluorescence. 2. Assignment of tryptophanyl residues of the carrier to the responses to specific ligands. *Biochemistry* **35,** 16125–16131
43. Majima, E., Shinohara, Y., Yamaguchi, N., Hong, Y. M., and Terada, H. (1994) Importance of loops of mitochondrial ADP/ATP carrier for its transport activity deduced from reactivities of its cysteine residues with the sulfhydryl reagent eosin-5-maleimide. *Biochemistry* **33,** 9530–9536
44. Majima, E., Yamaguchi, N., Chuman, H., Shinohara, Y., Ishida, M., Goto, S., and Terada, H. (1998) Binding of the fluorescein derivative eosin Y to the mitochondrial ADP/ATP carrier. Characterization of the adenine nucleotide binding site. *Biochemistry* **37,** 424–432
45. Kolarov, J., Kolarova, N., and Nelson, N. (1990) A third ADP/ATP translocator gene in yeast. *J. Biol. Chem.* **265,** 12711–12716
46. Chenna, R., Sugawara, H., Koike, T., Lopez, R., Gibson, T. J., Higgins, D. G., and Thompson, J. D. (2003) Multiple sequence alignment with the Clustal series of programs. *Nucleic Acids Res.* **31,** 3497–3500
47. Sanchez, J. F., Kauffmann, B., Grélard, A., Sanchez, C., Trézéguet, V., Huc, I., and Lauquin, G. J.-M. (2012) Unambiguous structure of atractyloside and carboxyatractyloside. *Bioorg. Med. Chem. Lett.* doi: 10.1016/j.bmcl.2012.02.040